Delft University of Technology

Urea-Functionalized Silver Catalyst toward Efficient and Robust CO$_2$ Electrolysis with Relieved Reliance on Alkali Cations

Garg, Sahil; Li, Mengran; Hussain, Tanveer; Idros, Mohamed Nazmi; Wu, Yuming; Zhao, Xiu Song; Wang, Geoff G.X.; Rufford, Thomas E.

Important note
To cite this publication, please use the final published version (if applicable).
Please check the document version above.

Urea-functionalized silver catalyst towards efficient and robust CO$_2$ electrolysis with relieved reliance of alkali cations

Sahil Garg[a,b], Mengran Li[a,c,*], Tanveer Hussain[a,d], Mohamed Nazmi Idros[a], Yuming Wu[a], Xiu Song Zhao[a], Geoff G.X. Wang[a], Thomas E. Rufford[a,*]

[a] *School of Chemical Engineering, the University of Queensland, St Lucia, 4072, Brisbane, Queensland, Australia*

[b] *Department of Physics, Technical University of Denmark, 2800 Kgs. Lyngby, Denmark*

[c] *Department of Chemical Engineering, Faculty of Applied Sciences, Delft University of Technology, van der Maasweg 9, 2629 HZ Delft, The Netherlands*

[d] *School of Science and Technology, University of New England, Armidale, New South Wales 2351, Australia*

Corresponding authors: M. Li m.li6@uq.edu.au; T.Rufford email t.rufford@uq.edu.au

Abstract

We report a new strategy to improve the reactivity and durability of a membrane electrode assembly (MEA) type electrolyser for CO$_2$ electrolysis to CO by modifying the silver catalyst layer with urea. Our experimental and theoretical results show that mixing urea with the silver catalyst can promote electrochemical CO$_2$ reduction (CO$_2$R), relieve limitations of alkali cation transport from the anolyte, and mitigate salt precipitation in the gas diffusion electrode in long term stability tests. In a 10 mM KHCO$_3$ anolyte, the urea-modified Ag catalyst achieved CO selectivity 1.3-times better with energy efficiency 2.8-fold better than an untreated Ag catalyst, and operated stably at 100 mA cm^{-2} with a Faradaic efficiency for CO above 85% for 200 h. Our work provides an alternative approach to fabricating catalyst interfaces in MEAs by modifying the catalyst structure and local reaction environment for critical electrochemical applications such as CO$_2$ electrolysis and fuel cells.

Keywords: CO$_2$ utilisation; urea; electrocatalyst; silver nanoparticles; vapour-fed electrolyser; membrane-electrode assembly

1 Introduction

Electrochemical CO_2 reduction (CO_2R) technologies show promise to convert CO_2 to chemical feedstocks and fuels using renewable electricity.[1, 2] Of the various designs for CO_2 electrolysers, membrane electrode assembly (MEA) designs, or zero-gap electrolysers, are emerging as one of the CO_2R technologies that can achieve high product selectivity at high current densities.[3-9] A core advantage of MEA electrolysers is that these designs do not have bulk, flowing catholyte between the cathode and the ion exchange membrane, which significantly reduces ohmic losses in the electrolyser and thus enhances the overall energy efficiency of CO_2R.[9] However, the absence of catholyte can also lead to poor stability due to salt precipitation in the cathode gas diffusion electrode (GDE) and if there are insufficient alkali cations available at the cathode the CO_2R selection may be reduced.[6, 10, 11] Both these issues originate from the strong reliance of MEA electrolysers on alkali cations (e.g., K^+) for an active CO_2R[10].

Only a few engineering solutions have been reported to resolve these critical issues, including (i) using pure water as anolyte with the periodic injection of salt solutions to the cathode[5], (ii) periodic flushing the GDE with pure water to wash away the salts[6], or (iii) alternating cell voltages to minimize OH^- concentration at the interface.[12] However, these approaches all involve unsteady-state and periodic interventions that disrupt the electrolyser operations, which lead to poor overall process efficiency, increased complexity of process control infrastructure, and increased costs.

An alternative approach that is yet to be fully explored is to promote the CO_2R catalyst with molecular modifiers such as urea or ionic liquids.[13-18] There is evidence that urea or ionic liquids can influence the catalyst activity and selectivity through optimizing catalyst structures and local reaction environments. These modifier molecules can have effects such as (i) stabilizing CO_2R reaction intermediate species such as *COOH,[19, 20] (ii) altering catalyst local proton availability by increasing hydrophobicity or decreasing dielectric constant in the electric double layer,[21-24] (iii) optimizing the catalyst electronic structure for CO_2R,[20, 25] and (iv) restructuring the catalyst surface to allow exposure of more active sites for CO_2R and increase of local pH to suppress HER.[26] We expect that these molecules to promote the catalytic activity in the MEA cells while reducing their dependency on alkali cations.

In this study, immobilized urea in the silver catalyst layer of the cathode GDE in MEA electrolyser by mixing the urea with the silver nanoparticles before catalyst deposition (**Figure S1**). We chose urea in this work because, in our earlier work with catholyte-fed electrolysers[18], urea proved effective to modify the Ag surface and promote CO_2R to CO. In this paper we report that the inclusion of urea in the catalyst layer enabled the MEA to operate efficiently with a dilute 10 mM $KHCO_3$ anolyte. Our experimental and theoretical results unveil that the amino group ($-NH_2$) of urea can bind strongly with the silver surface, which could promote CO_2R performance by stabilizing the *COOH intermediate and suppressing hydrogen evolution reaction (HER). Consequently, the urea-modified cathode achieved a stable FE_{CO} above 85% at 100 $mA \cdot cm^{-2}$ for 200 h in an MEA configuration with 10 mM $KHCO_3$ as the anolyte. Our work demonstrates an alternative approach to circumvent the long-lasting issues of MEA-based electrochemical processes by modifying the catalyst structures and local reaction environment with molecular modifiers.

2　Methods

2.1　Preparation of catalyst ink and gas diffusion electrodes

We prepared several Ag-based gas diffusion electrodes (GDE) with different catalyst inks. The benchmark catalyst ink had 100 mg of Ag nanoparticles (NPs, 20-40 nm) from Alfa Aesar mixed with 100 µL of polytetrafluoroethylene (PTFE, 60wt% dispersion in water diluted to 6 wt%), and 8 mL of isopropyl alcohol (IPA, ≥ 99.7%, Sigma-Aldrich). The catalyst ink was sonicated for 30 min and then deposited onto a commercial gas diffusion layer (GDL 240, Fuel Cell Store) by spray-coating (RS pro airbrush kit, RS components) until an Ag catalyst loading of 1 ± 0.05 $mg \cdot cm^{-2}$ was achieved. We refer to this benchmark, untreated Ag based cathode as the Ag-GDE (**Figure S1**).

We prepared urea modified Ag GDEs using urea (≥ 99.5% Sigma Aldrich) by two different methods. In method 1, the Ag-U-layered GDE (**Figure S1**) was prepared by spary-coating a solution of 1 g of urea in 4 mL of water and 4 mL of IPA onto the already prepared Ag GDE to achieve a 0.5 ± 0.05 $mg \cdot cm^{-2}$ loading of urea. In method 2, Ag-U-mixed GDE was prepared by mixing 100 mg of Ag NPs, 50 mg of urea pellets and 100 µL of PTFE (6 wt% in water) in 4 mL of water and 4 mL of IPA. This mixture was sonicated for 30 mins then spray coated directly on the GDL 240. The total loading of ink on Ag-U-mixed GDE was 1.5 ± 0.05 $mg \cdot cm^{-2}$ to achieve a silver loading of 1 $mg \cdot cm^{-2}$ and urea loading of 0.5 $mg \cdot cm^{-2}$. Prior work by

3

others[27] used similar "layered" and "mixed" methods with multi-walled carbon nanotubes and the Ag catalyst for CO_2R. Although the spray-coating methods in our study is similar to that prior work, the role of urea is not the same as the carbon nanotubes because (1) urea serves as a molecular modifier to limit proton availability and strengthen binding with CO_2R intermediates, and (2) the water is limited at the catalyst-membrane interface so that a high concentration of urea can be maintained close to the catalyst surface.

2.2 CO_2 electrolyser assembly and operation

We purchased a 5 cm^2 CO_2 electrolyser from Dioxide Materials (USA) (**Figure S2**) with a humified CO_2 gas chamber, and an anolyte chamber with a IrO_2-based GDE (Dioxide Materials). We pumped 10 mM $KHCO_3$ ($\geq$ 99.5%, Sigma-Aldrich) at a rate of 1 ml·min^{-1} through the serpentine flow-field of the anode-side endplate. The anode and cathode were separated by an anion-exchange membrane (AEM Sustainion®, X37-50 grade, Dioxide Materials). Humidified CO_2 at temperature = 20 ± 3 ºC was supplied to the cathode GDE at a flow rate of 60 sccm (unless stated otherwise) using a mass flow controller (pMFC, MKS instruments, ± 1% precision). The catalyst layers on the anode and cathode each faced towards the AEM.

Electrochemical measurements were conducted at ambient temperature and pressure using an Autolab PGSTAT302N potentiostat in a two-electrode configuration. The CO_2 electrolyser was tested using a galvanostatic mode at current densities (CD) from 25 to 200 mA·cm^{-2}. The flow rate of the effluent gas (unreacted CO_2 + gas products) from the cathode cell was measured with a digital flowmeter (Optiflow 520, Sigma-Aldrich, ± 3% resolution). At each CD, the gas products were analyzed using a gas chromatograph (GC 2030, Shimadzu) equipped with a thermal conductivity detector (TCD), flame ionization detector (FID), and a packed column (Shincarbon). The first gas sample was analyzed after 500 s or when the cell voltage becomes stable (whichever was later). At least three different gas injections were analyzed at regular intervals, and an average value was reported. We report all cell voltages here as the average cell potential recorded over time intervals of at least 100 s at each CD. No iR-correction was applied to the reported voltages values. Ohmic and charge transfer resistance was determined by galvanostatic electrochemical impedance spectroscopy (EIS) at frequencies ranging from 100 kHz to 1 Hz, recording 2 times per decade.

The faradaic efficiency (FE) of the gaseous products (P) were determined using the following equation:

$$FE_p = \frac{z_P \cdot F \cdot N_P}{I} \times 100 \tag{1}$$

where z_P is the number of electrons required for a given product (P); F is Faraday's constant; N_P is the molar flow rate of the gases product calculated from the GC and the effluent gas flow rate; and I is the current applied.

The energy efficiency (EE_{CO}) of CO_2R to CO was calculated using the following equation:

$$EE_{CO} = \frac{FE_{CO} \cdot E_{eq,cell}}{E_{cell}} \tag{2}$$

where $E_{eq,cell}$ is standard cell potential (-1.34 V) for CO_2R to CO coupled with the O_2 evolution reaction at the anode and E_{cell} is the actual cell potential.

For the long-term electrode durability test, a constant current density of 100 mA·cm^{-2} was applied across the electrolyser. The cell potential was monitored and the FE_{CO} was calculated every 1 h.

2.3   Characterisation

Scanning electron microscopy (SEM) of GDEs before and after CO_2R experiments was performed on JOEL JSM-7100 or JSM-7001 field emission microscope. X-ray photoelectron spectroscopy (XPS) was obtained with a Kratos Axis Ultra XPS spectrometer using a monochromatic Al Kα radiation (1486.6 eV) source for excitation. CASA® software was used to process and calibrate all the XPS spectra using carbon (C) 1s peak to 284.6 eV. Raman data were collected using a Renshaw Raman microscope equipped with 514 nm and 785 nm laser. Raman measurements were acquired using a 514 nm laser (unless stated otherwise) and the laser power was regulated between 10 to 100 mW to acquire sufficient signals for the spectra. We used Spectragryph software for analysis and baseline correction for all the Raman Spectra.

3   Results and discussions

3.1   Performance of MEA cells with urea-embedded silver catalyst

Figure 1A and B show the Faradaic efficiencies of H_2 (FE_{H2}) and CO (FE_{CO}) of the MEA electrolysers with the untreated Ag GDE, Ag-U-mixed GDE, and Ag-U-layered GDE. We repeated each test at least three times and report the mean FE_P values with error bars showing the standard deviation. As shown in **Figure 1A and 1B**, the Ag-U-mixed cell shows a significant improvement of FE_{CO} and suppression of unwanted HER at higher current densities. For example, at CD of 150 mA·cm^{-2}, the Ag-U-mixed GDE achieved a FE_{CO} of 71.86 ± 0.09%, which is far higher than for the untreated Ag GDE (FE_{CO} = 50.81 ± 2.43%) and the Ag-U-layered GDE (FE_{CO} = 35.55 ± 4.90%). The FE_{H2} remains below 10% for the Ag-U-mixed GDE but was up to FE_{H2} = 40% at 200 mA·cm^{-2} for the untreated Ag GDE. The HER is the dominant reaction for the Ag-U-layered cells, where the FE_{CO} is the lowest among the cell tests. The large difference in CO_2R selectivity to CO between Ag-U-mixed and Ag-U-layered cells indicates urea may have a critical effect on the local reaction environment and or state of the Ag catalyst at the active sites.
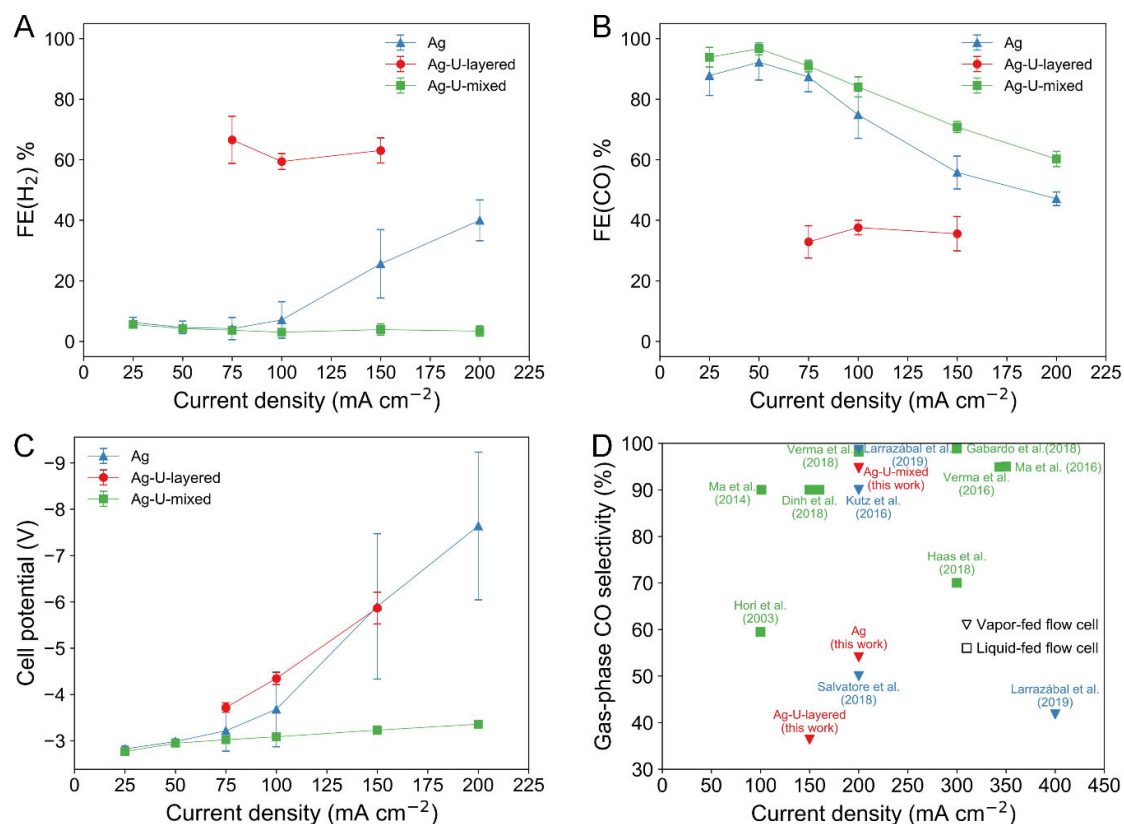
Figure 1. Comparison of faradaic efficiency of (A) H_2; (B) CO; and (C) cell potentials for CO_2 electrolysis in MEA electrolyser using Ag GDE, Ag-U-layered GDE, and A-U-mixed GDE with equivalent of 1 ± 0.05 mg cm^{-2} Ag loadings. Error bars show a standard deviation of three separate experiments. (D) the landscape of current density vs CO selectivity in gaseous products for liquid-fed flow electrolysers and vapor-fed electrolysers (MEA electrolysers) with Ag-based cathodes. We only include here results reported at a total current density higher than 100 mA·cm^{-2}. The details of the literature presented in (D) are provided in Table S1 of the Supplementary Information.

Additionally, the total faradaic efficiency (CO + H_2) decreases with current density in Ag-U-mixed cells (**Figure S3**). We anticipate that the loss of faradaic efficiencies in both Ag-U-mixed and Ag cells at high rates may relate to crossover of formate ions through the AEM and subsequent oxidation of the formate ions at the anode.[28, 29] We confirmed trace concentrations of formate ions in the anolyte by NMR after the CO_2R test (**Figure S4**). We also ruled out the decomposition of urea to CO, or CO_2, as a contributor to the FE_{CO} results by performing electrolysis with an Ag-U-mixed GDE fed with argon gas. **Figure S5** shows that in the absence of a CO_2 gas feed we observed 100% FE_{H2}, and from this we infer that urea did not decompose to CO at the conditions used for CO_2R. This control experiment also confirms that the increase in FE_{CO} over Ag-U-mixed cells during CO_2R only originates from the reduction of CO_2.

7

Figure 1C shows clearly that the urea in the GDE catalyst layer has a profound impact on the overall cell potentials. The cell potentials of Ag-U-mixed GDE electrolyser increase from 2.789 ± 0.055 V at 25 mA·cm^{-2} to 3.359 ± 0.048 V at 200 mA·cm^{-2}, and these cell potentials are much lower than for the untreated Ag GDE (7.640 ± 1.594 V at 200 mA·cm^{-2}). We note that 7.640 V uis a relatively large cell potential here, and this result is partly because of the low concentration anolyte (0.1 mM) used in these experiments. This observation further highlights the significance of the cell potentials observed for the Ag-U-mixed GDE and suggests that in addition to the effects on CO$_2$R selectivity the urea also affects the required overpotentials at high current densities. The significance of this result is that the overall CO$_2$ conversion energy efficiency of the electrolyser improved from 8.60 ± 1.88 % in untreated Ag cells to 24.04 ± 1.11 % in Ag-U-mixed cells at 200 mA·cm^{-2} (**Figure S6**).

Figure 1D and **Table S1** summarize a few recent reports of CO selectivity in the gaseous products (CO + H$_2$) in vapor-fed MEA electrolysers and liquid-fed electrolysers. Although the Ag-U-mixed cell performance is not at the top right corner of **Figure 1D** (i.e., a high CO selectivity in gaseous products at high current densities), our result ranks among the highest reported CO selectivity in the gaseous products at high current densities reported in an MEA electrolyser.

By varying catalyst loading from 0.75 mg·cm^{-2} to 1.5 mg·cm^{-2} for the Ag-U-mixed cells, as shown in **Figure S7**, we observed no discernable changes of cell potentials and FE$_{H2}$ when changing catalyst loading. There is only a slightly lower FE$_{CO}$ for 0.75 mg·cm^{-2} than 1.5 mg·cm^{-2}, which results from the reduced number of active sites for CO$_2$R. The FE$_{H2}$ of all the Ag-U-mixed cells with different catalyst loadings remain lower than the untreated Ag cells (see **Figure S7** and **Figure 1A**), further confirming the effective role of urea in suppressing HER in the MEA cells using 10 mM KHCO$_3$.

3.2 The role of urea in catalyst activation for CO$_2$R

Our previous work reported that urea can be specifically adsorbed on the Ag surface and enhances CO production by stabilizing the CO$_2$R intermediates.[18] Therefore, in the Ag-U-mixed GDE, we believe the urea may interact strongly with the Ag catalyst and promote efficient CO$_2$ reduction. We examined the surface of the catalyst layer of untreated Ag and Ag-U-mixed samples visually and with XPS. We observed the Ag-U-mixed GDE is darker compared to the untreated Ag GDE, and the urea modified catalyst layer had a greenish tinge

8

(**Figure 2A**). The uniform distribution of Ag nanoparticles from SEM images (**Figure S8**) indicatea the color difference is not from differences in the morphology. Instead, the XPS data show the colour change is due to chemical interactions. The Ag 3d XPS spectra in **Figure 2B** for the Ag-U-mixed electrode exhibit two distinctive deconvoluted peaks at 368.4 eV[30] and 369.5 eV[31], which correspond to the features of Ag and Ag-organic amine, respectively. In contrast, the Ag 3d spectra for the Ag electrode only show a single Ag metallic peak at 368.4 eV. The presence of an Ag-organic amine peak suggests bonding between the Ag surface and the amino groups of the urea.
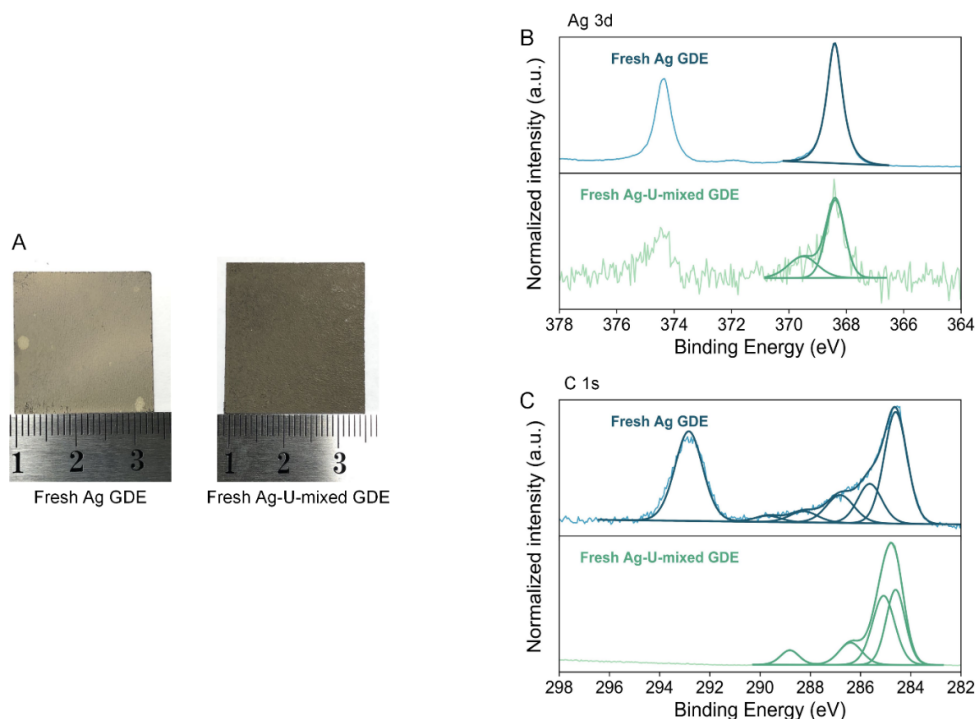

Figure 2. Images of freshly prepared (A) Ag electrode and Ag-U-mixed electrode; high-resolution XPS spectra of (B) Ag 3d and (C) C 1s on the fresh Ag and fresh Ag-U-mixed electrodes. The raw spectra are shown with light-colored lines, while the analogous fitted and deconvoluted peaks are shown with the dark-colored lines.

The C 1s spectra of Ag electrode has deconvoluted peaks for graphitic carbon at 284.6 eV;[32] carbon contamination at 285.6, 286.8, and 288.3 V;[32, 33] and fluorinated carbons at 289.7 and 292.8 eV (due to PTFE in the catalyst layer).[34, 35] However, the Ag-U-mixed GDE exhibits two additional peaks at 286.3 and 288.7 eV, corresponding to $C-NH_2$ and $C=O$, respectively. [36] The atomic percentages of $C-NH_2$ and $C=O$ on the Ag-U-mixed surface are 13.57 and 7.14 (almost 2:1 ratio), which is in good agreement with the 2:1 ratio of $-NH_2$ and $C=O$ groups in the urea.

The N 1s XPS peaks of Ag-U-mixed GDE (shown in **Figure S9**) at 399.2 and 400.0 eV can be assigned to $C-NH_2$[36] and Ag-organic amine, [37] respectively.

The C1s and Ag 3d XPS data confirm the availability of urea on the Ag-U-mixed electrode surface and its chemical interactions with the Ag catalyst. The availability of urea in Ag-U-mixed GDE may enable stabilisation of CO_2 electrolysis intermediate species and suppress HER (**Figure 1A**). Several groups such as Ahn et al.[38] and Cao et al.[39] reported that amino groups on the electrode surface facilitate the stabilization of CO_2R intermediates (e.g. *COOH) through hydrogen bonding, and thereby improving the CO_2R performance. In addition, Kim et al.[19] proposed that the adsorbed amine molecules on the Ag can destabilize the *H binding, which inhibits the HER.

Characterisation of the catalyst layers by XPS after CO_2R may provide further information about the interactions during CO_2R. Unfortunately, XPS of used catalyst from an MEA electrolyser is unlikely to be useful in this case because the intimate contact of catalyst layer and membrane in the MEA leads to delamination of the Ag-U-mixed catalyst when the electrolyser is dissembled (see **Figure S10**). Instead, we used Raman spectroscopy to compare the interactions between urea and Ag nanoparticles in the Ag-U-mixed GDE to spectra of urea, PTFE, bare GDL 240, the Sustainion AEM, and a preparation of the catalyst ink (**Figure 3A**). The fresh urea powder has several distinctive peaks at 548, 1011, 1541, 1581, and 1649 cm^{-1}, corresponding to N-C-N bending mode,[40] N-C-N symmetric stretching mode,[40] $-NH_2$ bending mode,[40] H-bonded C=O stretching mode,[40] and H-free C=O stretching mode,[40] respectively. The fresh urea powder has three additional peaks at 3245, 3355, and 3437 cm^{-1}, which are relevant to the anti-symmetric and symmetric $-NH_2$ stretching modes. These peak frequencies agree with the literature data.[40, 41]

The urea-related peaks in the fresh Ag-U-mixed electrode are positioned at 548, 1001, 1558, 1592, 3216, 3366, and 3459 cm^{-1}. A slight shift of urea peaks in the fresh Ag-U-mixed GDE may be attributed to the interaction of urea with the Ag.[42] Similarly, we observed the urea-related peaks in the dried Ag-U-mixed catalyst ink (fresh), used Ag-U-mixed electrode, and the used AEM with catalyst layer stuck on it after the CO_2R (see **Table S2** in the supporting information). However, we only observed very small $-NH_2$ anti/symmetric and symmetric stretching mode peaks over either the used Ag-U-mixed electrode or the used AEM. The low

intensity of -NH$_2$ stretching mode might be related to the low availability of urea left on the used Ag-U-mixed GDE after the CO$_2$R test.

Interestingly, in all the samples that contained urea and Ag we observed a Raman peak at around 230 cm^{-1} that was not observed in the urea powders, GDL 240, PTFE, or the AEM. This new peak is likely attributed to the Ag-urea vibrations, indicating chemisorption of urea on the Ag surface.[43] This analysis by Raman provides further evidence of strong interactions between urea and Ag through a Ag-amino group.
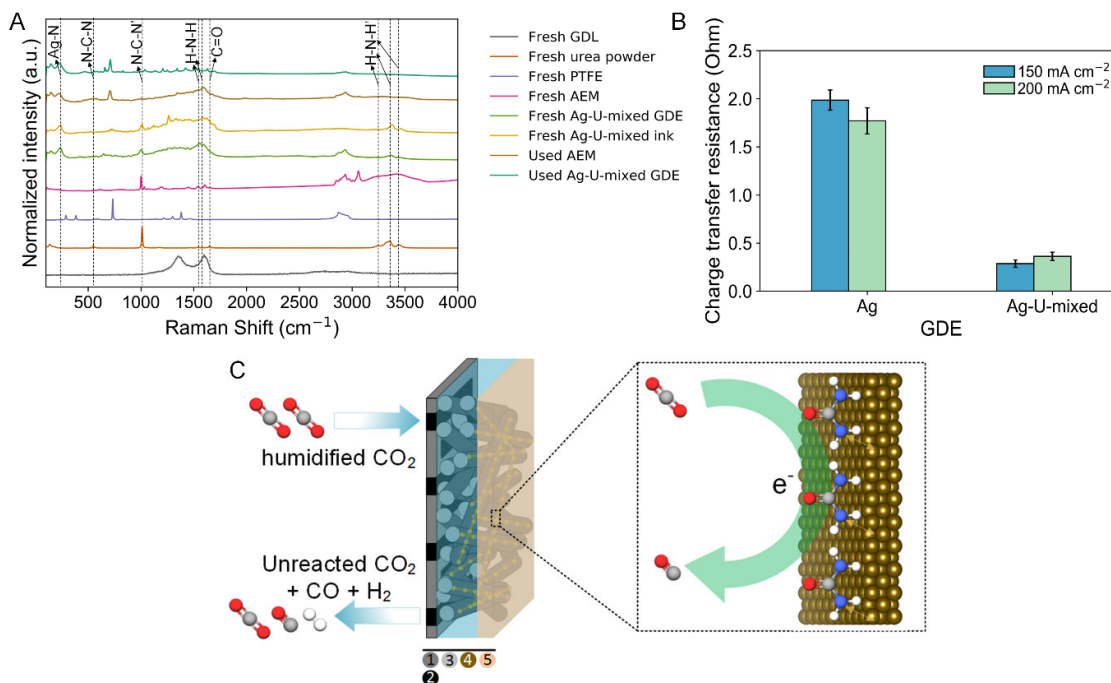

Figure 3. (A) Comparison of Raman spectra of different species including fresh GDL, fresh urea powder, fresh PTFE, fresh AEM, fresh Ag-U-mixed, fresh Ag-U-mixed ink (dried in the air), used Ag-U-mixed AEM, and used Ag-U-mixed electrode; (B) Charge transfer resistances by modeling impedance experiments during CO$_2$R in Ag and Ag-U-mixed electrodes. The charge transfer resistance shown may be attributed to both the cathode and anode; and (C) an illustration of the cathode part of the MEA in which the availability of urea could help stabilize the CO$_2$R intermediates, where 1 is endplate, 2 is gas flow-field, 3 is gas diffusion layer (GDL), 4 is the catalyst layer, and 5 is the membrane. Atom colors in (C) are O in red, C in grey, N in blue, and H in white.

We used electrochemical impedance spectroscopy (EIS) to investigate the overall resistance and charge transfer resistances of Ag and Ag-U-mixed cells at different current densities. This EIS method follows similar approaches for MEA-based devices reported in the literature.[5, 44] The high frequency intercept of the EIS curves shown in **Figure S11** (see experimental and fitted Nyquist plots) shows the overall cell resistance, while the semicircle represents the charge transfer resistance of both the cathodic and anodic half cell reactions. **Figure S11** shows slightly higher cell resistance in Ag-GDE than in Ag-U-mixed GDE at 200 mA·cm^{-2}, meaning that the availability of urea at the cathode-membrane interface promotes ion transport across the AEM. In **Figure 3B**, the charge transfer resistance (R_{CT}) calculated from the EIS is significantly larger in the Ag GDE than the Ag-U-mixed GDE. Although the R_{CT} data shown in **Figure 3B** accounts for resistances at both the cathode and the anode, we used the same type of anode (fresh each time) in each experiment so here decrease in R_{CT} for the Ag-U-mixed electrode can only be due to the change in the cathode. The trend of R_{CT} values in both Ag and Ag-U-mixed GDEs are consistent with the cell potential data in **Figure 1C**, meaning that a high R_{CT} increases the cell potential. The large R_{CT} for untreated Ag GDE may result from an insufficient availability of K^+ ions at the cathode for efficient CO$_2$R, which is known to be an issue when using dilute anolytes. In contrast, we propose that the lower R_{CT} for Ag-U-mixed GDE observed with the same dilute anolyte may relate to urea enhancing CO$_2$R on the Ag catalyst surface. (**Figure 3C)**

We tested this hypothesis on the role of urea in promoting CO$_2$R using density functional theory (DFT) simulations. A detailed description of the DFT calculations is provided in the Supporting Information. Considering the Ag catalyst in our study is mainly dominated by the Ag(111) facets (see **Figure S12**), we used a periodic Ag(111) surface with seven layers and 112 Ag atoms (named as Ag$_{112}$) as our DFT model. The modeling identified that the urea molecules can strongly interact with Ag(111) by sitting in a horizontal orientation on Ag(111) surface with a urea-Ag$_{112}$ binding energy of -0.68 eV and a binding distance of 2.86 Å. (see **Figure S13**) This finding is consistent with our experimental observations from XPS and Raman spectroscopy.

CO$_2$ electrolysis to CO is reported to proceed via successive proton-coupled electron transfer (PCET) steps associated with the formation of *CO and *COOH intermediates.[45, 46] We, therefore, calculated the binding energies, minimum binding distances, and Gibbs free energies of the key intermediates in CO$_2$R and HER (including *H, *CO, and *COOH) over the

optimized Ag_{112} structure (see **Figure S14** and **S15**) with and without urea adsorption. The DFT results summarized in **Table S3** show that the urea-adsorbed Ag structure has a Gibbs binding energy 17% higher with *COOH and 15.3% higher with *CO as compared with the bare Ag structure. A strengthened interaction with *COOH relative to that with *CO could contribute to the enhancement of CO_2R to CO as observed from the experiment (**Figure 1**). Our conclusion here that amino group stablize the reaction intermediates are consistent with the literature.[10] Moreover, we found only a small difference in the Gibbs binding energies with *H for urea-adsorbed Ag (-1.47 eV) and bare Ag (-1.45 eV), meaning that the urea shows negligible thermodynamic effect in inhibiting HER. In this case, the experimentally observed HER suppression by urea nay be due to other effects of urea on the local reaction environment at the cathode, such as influence local pH.

Direct measurement of local pH in the MEA electrolyser is not feasible, and prediction of local pH by simulations is computationally intensive and uncertain. However, we can make relative inferences about local pH conditions for the untreated Ag GDE and the Ag-U-mixed GDE from the rate of carbonate formation from the reaction of acidic CO_2 with OH^- during high current density CO_2 electrolysis. We estimated at 200 mA·cm^{-2} current density there was about 5% more CO_2 loss to carbonate with the Ag-U-mixed GDE than with the untreated Ag GDE (see **Table S4**), which suggests the local pH for Ag-U-mixed GDE will be higher. The higher local pH limits proton availability and thus suppresses the HER. We caution that our CO_2 carbonation calculations using these experimental data can provide only a relative indication of local pH conditions. We also acknowledge that CO_2 loss via carbonation is a critical challenge for CO_2 electrolysis that needs to be addressed, for example, by introducing protons or optimizing mass transport of water, ions, and gases.[11, 47]

3.3 Long-term electrolyser stability test

We tested the CO_2R performance and stability of Ag-U-mixed MEA for 200 h at a constant current density of 100 mA·cm^{-2} with no operational interruptions during the test. The cell was again supplied with 10 mM $KHCO_3$ anolyte throughout the stability tests. In these tests, the initial FE_{CO} of 91% dropped to about 85% in the first 25 h test, then the selectivity remained stable at 85% for the remaining 175 h of the test (**Figure 4A**). The FE_{H2} slowly increased with time but kept below 5% across the test. The CO selectivity loss in the first 25 h is likely due to the flooding of the catalyst from the loss of electrode wettability under applied potential.[48] The

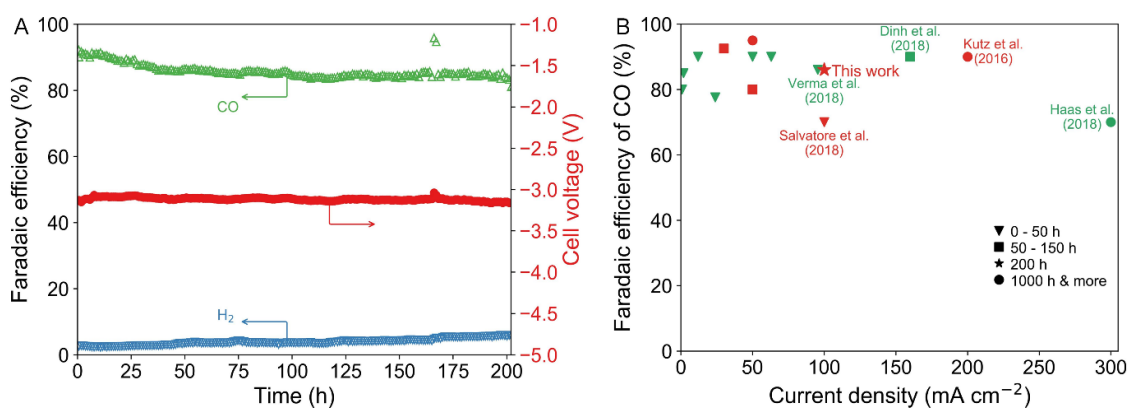MEA cell maintained a relatively constant cell voltage of 3.116 ± 0.019 V over the durability test.

Figure 4. (A) Faradaic efficiency of CO and H₂ and cell voltage as a function of time for 200 h CO₂R durability test at a constant current density of 100 mA·cm⁻² (cathode: Ag-U-mixed GDE; anode: IrO₂-based GDE; catholyte: humidified CO₂ at 60 sccm, anolyte: 10 mM KHCO₃ at 1 ml/min; and membrane: Sustainion AEM). (B) summary of long-term electrode durability test showing the faradaic efficiency of CO as a function of current density over various catalysts tested in liquid-fed flow cells (green color), and MEA cells (red color). The details of the literature work shown in (B) are provided in Table S3.

After 200 h operation, the selectivity of CO dropped from 85% to 74% in a sharp decline (**Figure S16A**) due to potassium bicarbonate (KHCO₃) precipitation in part of the gas flow field (see **Figure S16B**).[5] The salt precipitation is due to (i) the K⁺ diffusion through the AEM from the anolyte, (ii) limited water at the cathode, and (iii) the limited solubility of the carbonates.[6, 29] We ruled out the potential contribution from the Ag deactivation because there is nearly no difference in the Ag 3d XPS spectra (see **Figure S18**) of the Ag-U-mixed electrodes before and after the stability test, which excludes the contribution from catalyst deactivation. Instead, we observed a rapid drop of effluent flow rate from the cell after the 200 h test, where the degradation of FE$_{CO}$ follows a very similar trend. (**Figure S17**) The decreased flow rate reflects the blockage of CO₂ flow due to the salt precipitation.

We also did a long-term stability test with untreated Ag-GDE in our other work[49] (also shown in Figure S19), and found that the selectivity of CO was only around 62%, much less than to what we observed with Ag-U-mixed GDE (85%). In addition, the electrocatalytic performance cannot survive more than 100 h over Ag-GDE, while Ag-U-mixed GDE can run stably for almost double the time.

Although we had salt precipitation in the Ag-U-mixed GDE after the 200 h operation, the rate of salt precipitation, and its impact on electrolyser stability, was much slower than without the urea. These results demonstrated that the urea modified GDE can slow the salt precipitation process and enable highly selective and efficient CO_2R when using a dilute anolyte because the urea reduces the reliance of the electrolyser on transport of alkali cations to the cathode. **Figure 4B** compares our results with stability tests reported for CO_2R to CO electrolyser – including liquid-fed flow cells and vapour-fed MEA cells. The data are listed in **Table S5** (where we also include additional examples rom H-cell tests). The Ag-U-mixed cell outperforms most of the reported catalysts in terms of current density, energy efficiency, and CO_2R test time while sustaining the high FE_{CO}.

4   Conclusion

We demonstrated an alternative approach to improve both efficiency and stability of CO_2 electrolysis based on MEA cells by enhancing CO_2R and relieving the catalyst reliance on alkali cations. Our experiment and DFT calculations unveiled that the urea molecule can promote CO_2R by stabilizing *COOH at the silver surface and optimizing the local reaction environment to minimize HER. As a result, the urea-modified GDE demonstrated a notable improvement of CO_2R performance of the MEA cells with 10 mM $KHCO_3$ as the anolyte, with a 1.3-fold enhancement of CO selectivity at above 150 mA cm^{-2} and a 2.8-fold improvement of energy efficiency at 200 mA cm^{-2} as compared to bare Ag GDE. The cell could also maintain a continuous stable operation at 100 mA cm^{-2} for 200 h. Our work can be anticipated as a starting point to address the long-lasting issues faced by MEA-based technologies by modifying the catalyst interfaces and local reaction environment with molecular additives.

Supporting Information

The Supporting Information is available free of charge at https://pubs.acs.org/doi/10.1021/XX

- Description of density functional theory calculations including Binding and Gibbs free energy calculations, schematic of how different Ag GDEs were examined in this work, schematic representation of the electrolyser, formate detection using NMR, selectivity of H_2 while performing Ar electrolysis, energy efficiency plot, catalytic performance over different loadings of Ag-U-mixed GDEs, SEM data, high-resolution XPS data, photographs of Ag-U-mixed GDE and membrane - before and after CO_2R, Impedance

data, XRD data, optimized structures (with top and side views) of urea@Ag112 and pristine Ag used in DFT calculations, photo of salt precipitation in the cathode flow field, dependency of outlet cathode flowrate on selectivity of CO, long-term stability data using Ag-GDE, tables showing summary of literature reports, raman data, Binding and Gibbs free energies data, CO_2 carbonation data, summary of long-term stability tests in literature.

References

1. Spurgeon, J. M.; Kumar, B. A Comparative Technoeconomic Analysis of Pathways for Commercial Electrochemical CO_2 Reduction to Liquid Products. *Energy & Environmental Science* **2018**, *11* (6), 1536-1551. DOI: 10.1039/C8EE00097B.

2. Jouny, M.; Luc, W.; Jiao, F. General Techno-Economic Analysis of CO_2 Electrolysis Systems. *Industrial & Engineering Chemistry Research* **2018**, *57* (6), 2165-2177. DOI: 10.1021/acs.iecr.7b03514.

3. O'Brien, C. P.; Miao, R. K.; Liu, S.; Xu, Y.; Lee, G.; Robb, A.; Huang, J. E.; Xie, K.; Bertens, K.; Gabardo, C. M.; Edwards, J. P.; Dinh, C.-T.; Sargent, E. H.; Sinton, D. Single Pass CO_2 Conversion Exceeding 85% in the Electrosynthesis of Multicarbon Products via Local CO_2 Regeneration. *ACS Energy Letters* **2021**, *6* (8), 2952-2959. DOI: 10.1021/acsenergylett.1c01122.

4. Ozden, A.; Li, F.; García de Arquer, F. P.; Rosas-Hernández, A.; Thevenon, A.; Wang, Y.; Hung, S.-F.; Wang, X.; Chen, B.; Li, J.; Wicks, J.; Luo, M.; Wang, Z.; Agapie, T.; Peters, J. C.; Sargent, E. H.; Sinton, D. High-Rate and Efficient Ethylene Electrosynthesis Using a Catalyst/Promoter/Transport Layer. *ACS Energy Letters* **2020**, *5* (9), 2811-2818. DOI: 10.1021/acsenergylett.0c01266.

5. Endrődi, B.; Samu, A.; Kecsenovity, E.; Halmágyi, T.; Sebők, D.; Janáky, C. Operando Cathode Activation with Alkali Metal Cations for High Current Density Operation of Water-fed Zero-gap Carbon Dioxide Electrolysers. *Nature Energy* **2021**, *6* (4), 439-448. DOI: 10.1038/s41560-021-00813-w.

6. Endrődi, B.; Kecsenovity, E.; Samu, A.; Darvas, F.; Jones, R. V.; Török, V.; Danyi, A.; Janáky, C. Multilayer Electrolyzer Stack Converts Carbon Dioxide to Gas Products at High Pressure with High Efficiency. *ACS Energy Letters* **2019**, *4* (7), 1770-1777. DOI: 10.1021/acsenergylett.9b01142.

7. Kutz, R. B.; Chen, Q.; Yang, H.; Sajjad, S. D.; Liu, Z.; Masel, I. R. Sustainion Imidazolium-Functionalized Polymers for Carbon Dioxide Electrolysis. *Energy Technology* **2017**, *5* (6), 929-936. DOI: https://doi.org/10.1002/ente.201600636.

8. Ren, S.; Joulié, D.; Salvatore, D.; Torbensen, K.; Wang, M.; Robert, M.; Berlinguette, C. P. Molecular Electrocatalysts can Mediate Fast, Selective CO_2 Reduction in a Flow Cell. *Science* **2019**, *365* (6451), 367-369. DOI: 10.1126/science.aax4608.

9. Weng, L.-C.; Bell, A. T.; Weber, A. Z. Towards Membrane-electrode Assembly Systems for CO_2 Reduction: A Modeling Study. *Energy & Environmental Science* **2019**, *12* (6), 1950-1968, DOI: 10.1039/C9EE00909D.

10. Monteiro, M. C. O.; Dattila, F.; Hagedoorn, B.; García-Muelas, R.; López, N.; Koper, M. T. M. Absence of CO_2 Electroreduction on Copper, Gold and Silver Electrodes Without Metal Cations in Solution. *Nature Catalysis* **2021**, *4* (8), 654-662. DOI: 10.1038/s41929-021-00655-5.

11. Huang, J. E.; Li, F.; Ozden, A.; Sedighian Rasouli, A.; García de Arquer, F. P.; Liu, S.; Zhang, S.; Luo, M.; Wang, X.; Lum, Y.; Xu, Y.; Bertens, K.; Miao, R. K.; Dinh, C.-T.; Sinton, D.; Sargent, E. H. CO_2 Electrolysis to Multicarbon Products in Strong Acid. *Science* **2021**, *372* (6546), 1074-1078. DOI: 10.1126/science.abg6582.

12. Xu, Y.; Edwards, J. P.; Liu, S.; Miao, R. K.; Huang, J. E.; Gabardo, C. M.; O'Brien, C. P.; Li, J.; Sargent, E. H.; Sinton, D. Self-Cleaning CO_2 Reduction Systems: Unsteady Electrochemical Forcing Enables Stability. *ACS Energy Letters* **2021**, *6* (2), 809-815. DOI: 10.1021/acsenergylett.0c02401.

13. Tamura, J.; Ono, A.; Sugano, Y.; Huang, C.; Nishizawa, H.; Mikoshiba, S. Electrochemical Reduction of CO_2 to Ethylene Glycol on Imidazolium Ion-terminated Self-assembly Monolayer-modified Au Electrodes in an Aqueous Solution. *Physical Chemistry Chemical Physics* **2015**, *17* (39), 26072-26078, DOI: 10.1039/C5CP03028E.

14. Wang, W.; Ning, H.; Yang, Z.; Feng, Z.; Wang, J.; Wang, X.; Mao, Q.; Wu, W.; Zhao, Q.; Hu, H.; Song, Y.; Wu, M. Interface-induced Controllable Synthesis of Cu_2O Nanocubes for Electroreduction CO_2 to C_2H_4. *Electrochimica Acta* **2019**, *306*, 360-365. DOI: 10.1016/j.electacta.2019.03.146.

15. Zarandi, R. F.; Rezaei, B.; Ghaziaskar, H. S.; Ensafi, A. A. Electrochemical Reduction of CO_2 to Ethanol using Copper Nanofoam Electrode and 1-butyl-3-methyl-imidazolium Bromide as the Homogeneous Co-catalyst. *Journal of Environmental Chemical Engineering* **2019**, *7* (3), 103141. DOI: 10.1016/j.jece.2019.103141.

16. Khadhraoui, A.; Gotico, P.; Boitrel, B.; Leibl, W.; Halime, Z.; Aukauloo, A. Local Ionic Liquid Environment at a Modified Iron Porphyrin Catalyst Enhances the Electrocatalytic Performance of CO_2 to CO Reduction in Water. *Chem. Commun.* **2018**, *54* (82), 11630-11633, DOI: 10.1039/C8CC06475J.

17. Ummireddi, A. K.; Sharma, S. K.; Pala, R. G. S. Inhibition of Hydrogen Evolution Without Debilitating Electrochemical CO_2 Reduction via the Local Suppression of Proton Concentration and Blocking of Step-edges by Pyridine Functionalization on Cu Electrocatalysts. *Catalysis Science & Technology* **2021**, *11* (14), 4857-4865, 10.1039/D1CY00712B. DOI: 10.1039/D1CY00712B.

18. Garg, S.; Li, M.; Rufford, T. E.; Ge, L.; Rudolph, V.; Knibbe, R.; Konarova, M.; Wang, G. G. X. Catalyst–Electrolyte Interactions in Aqueous Reline Solutions for Highly Selective Electrochemical CO_2 Reduction. *ChemSusChem* **2020**, *13* (2), 304-311. DOI: 10.1002/cssc.201902433.

19. Kim, C.; Eom, T.; Jee, M. S.; Jung, H.; Kim, H.; Min, B. K.; Hwang, Y. J. Insight into Electrochemical CO_2 Reduction on Surface-Molecule-Mediated Ag Nanoparticles. *ACS Catalysis* **2017**, *7* (1), 779-785. DOI: 10.1021/acscatal.6b01862.

20. Kim, C.; Jeon, H. S.; Eom, T.; Jee, M. S.; Kim, H.; Friend, C. M.; Min, B. K.; Hwang, Y. J. Achieving Selective and Efficient Electrocatalytic Activity for CO_2 Reduction Using Immobilized Silver Nanoparticles. *Journal of the American Chemical Society* **2015**, *137* (43), 13844-13850. DOI: 10.1021/jacs.5b06568.

21. Buckley, A. K.; Lee, M.; Cheng, T.; Kazantsev, R. V.; Larson, D. M.; Goddard Iii, W. A.; Toste, F. D.; Toma, F. M. Electrocatalysis at Organic–Metal Interfaces: Identification of Structure–Reactivity Relationships for CO_2 Reduction at Modified Cu Surfaces. *Journal of the American Chemical Society* **2019**, *141* (18), 7355-7364. DOI: 10.1021/jacs.8b13655.

22. Barton Cole, E.; Lakkaraju, P. S.; Rampulla, D. M.; Morris, A. J.; Abelev, E.; Bocarsly, A. B. Using a One-Electron Shuttle for the Multielectron Reduction of CO_2 to Methanol: Kinetic, Mechanistic, and Structural Insights. *Journal of the American Chemical Society* **2010**, *132* (33), 11539-11551. DOI: 10.1021/ja1023496.

23. Banerjee, S.; Han, X.; Thoi, V. S. Modulating the Electrode–Electrolyte Interface with Cationic Surfactants in Carbon Dioxide Reduction. *ACS Catalysis* **2019**, *9* (6), 5631-5637. DOI: 10.1021/acscatal.9b00449.

24. Banerjee, S.; Zhang, Z.-Q.; Hall, A. S.; Thoi, V. S. Surfactant Perturbation of Cation Interactions at the Electrode–Electrolyte Interface in Carbon Dioxide Reduction. *ACS Catalysis* **2020**, *10* (17), 9907-9914. DOI: 10.1021/acscatal.0c02387.

25. Lim, H.-K.; Shin, H.; Goddard, W. A.; Hwang, Y. J.; Min, B. K.; Kim, H. Embedding Covalency into Metal Catalysts for Efficient Electrochemical Conversion of CO_2. *J. Am. Chem. Soc.* **2014**, *136* (32), 11355-11361. DOI: 10.1021/ja503782w.

26. Fang, Y.; Cheng, X.; Flake, J. C.; Xu, Y. CO_2 Electrochemical Reduction at Thiolate-modified Bulk Au Electrodes. *Catalysis Science & Technology* **2019**, *9* (10), 2689-2701, 10.1039/C9CY00506D. DOI: 10.1039/C9CY00506D.

27. Ma, S.; Luo, R.; Gold, J. I.; Yu, A. Z.; Kim, B.; Kenis, P. J. A. Carbon Nanotube Containing Ag Catalyst Layers for Efficient and Selective Reduction of Carbon Dioxide. *Journal of Materials Chemistry A* **2016**, *4* (22), 8573-8578, 10.1039/C6TA00427J. DOI: 10.1039/C6TA00427J.

28. Larrazábal, G. O.; Strøm-Hansen, P.; Heli, J. P.; Zeiter, K.; Therkildsen, K. T.; Chorkendorff, I.; Seger, B. Analysis of Mass Flows and Membrane Cross-over in CO_2 Reduction at High Current Densities in an MEA-Type Electrolyzer. *ACS Applied Materials & Interfaces* **2019**, *11* (44), 41281-41288. DOI: 10.1021/acsami.9b13081.

29. Li, Y. C.; Yan, Z.; Hitt, J.; Wycisk, R.; Pintauro, P. N.; Mallouk, T. E. Bipolar Membranes Inhibit Product Crossover in CO_2 Electrolysis Cells. *Advanced Sustainable Systems* **2018**, *2* (4), 1700187. DOI: https://doi.org/10.1002/adsu.201700187.

30. Hsieh, Y.-C.; Betancourt, L. E.; Senanayake, S. D.; Hu, E.; Zhang, Y.; Xu, W.; Polyansky, D. E. Modification of CO_2 Reduction Activity of Nanostructured Silver Electrocatalysts by Surface Halide Anions. *ACS Applied Energy Materials* **2019**, *2* (1), 102-109. DOI: 10.1021/acsaem.8b01692.

31. Xue, G.; Dai, Q.; Jiang, S. Chemical reactions of imidazole with metallic silver studied by the use of SERS and XPS techniques. *Journal of the American Chemical Society* **1988**, *110* (8), 2393-2395. DOI: 10.1021/ja00216a009.

32. Ren, L.; Yang, F.; Wang, C.; Li, Y.; Liu, H.; Tu, Z.; Zhang, L.; Liu, Z.; Gao, J.; Xu, C. Plasma Synthesis of Oxidized Graphene Foam Supporting Pd Nanoparticles as a New Catalyst for One-pot Synthesis of Dibenzyls. *RSC Advances* **2014**, *4* (108), 63048-63054, 10.1039/C4RA11060A. DOI: 10.1039/C4RA11060A.

33. Akhter, S.; Zhou, X. L.; White, J. M. XPS Study of Polymer/organometallic Interaction: Trimethyl Aluminum on Polyvinyl Alcohol Polymer. *Appl. Surf. Sci.* **1989**, *37* (2), 201-216. DOI: https://doi.org/10.1016/0169-4332(89)90483-2.

34. Strohmeier, B. R. Evaluation Of Polymeric Standard Reference Materials For Monitoring The Performance Of X-Ray Photoelectron Spectrometers. *Appl. Surf. Sci.* **1991**, *47* (3), 225-234. DOI: https://doi.org/10.1016/0169-4332(91)90036-J.

35. Hantsche, H. High Resolution XPS of Organic Polymers, the Scienta ESCA300 database. By G. Beamson and D. Briggs, Wiley, Chichester 1992, 295 pp., hardcover, £ 65.00, ISBN 0-471-93592-1. *Adv. Mater.* **1993**, *5* (10), 778-778. DOI: https://doi.org/10.1002/adma.19930051035.

36. Lee, T. H.; Rabalais, J. W. X-ray Photoelectron Spectra and Electronic Structure of Some Diamine Compounds. *J. Electron. Spectrosc. Relat. Phenom.* **1977**, *11* (1), 123-127. DOI: https://doi.org/10.1016/0368-2048(77)85052-4.

37. Thornburg, D. M.; Madix, R. J. Cleavage of NH Bonds by Active Oxygen on Ag(110): II. Selective Oxidation of Ethylamine to Acetonitrile. *Surf. Sci.* **1990**, *226* (1), 61-76. DOI: https://doi.org/10.1016/0039-6028(90)90154-Z.

38. Ahn, S.; Klyukin, K.; Wakeham, R. J.; Rudd, J. A.; Lewis, A. R.; Alexander, S.; Carla, F.; Alexandrov, V.; Andreoli, E. Poly-Amide Modified Copper Foam Electrodes for Enhanced Electrochemical Reduction of Carbon Dioxide. *ACS Catalysis* **2018**, *8* (5), 4132-4142. DOI: 10.1021/acscatal.7b04347.

39. Cao, Z.; Zacate, S. B.; Sun, X.; Liu, J.; Hale, E. M.; Carson, W. P.; Tyndall, S. B.; Xu, J.; Liu, X.; Liu, X.; Song, C.; Luo, J.-h.; Cheng, M.-J.; Wen, X.; Liu, W. Tuning Gold Nanoparticles with Chelating Ligands for Highly Efficient Electrocatalytic CO_2 Reduction. *Angewandte Chemie International Edition* **2018**, *57* (39), 12675-12679. DOI: 10.1002/anie.201805696.

40. Frost, R. L.; Kristof, J.; Rintoul, L.; Kloprogge, J. T. Raman Spectroscopy of Urea and Urea-intercalated Kaolinites at 77 K. *Spectrochimica Acta Part A: Molecular and Biomolecular Spectroscopy* **2000**, *56* (9), 1681-1691. DOI: https://doi.org/10.1016/S1386-1425(00)00223-7.

41. Keuleers, R.; Desseyn, H. O.; Rousseau, B.; Van Alsenoy, C. Vibrational Analysis of Urea. *The Journal of Physical Chemistry A* **1999**, *103* (24), 4621-4630. DOI: 10.1021/jp984180z.

42. Ferraro, J. R.; Nakamoto, K.; Brown, C. W. Chapter 1 - Basic Theory. In *Introductory Raman Spectroscopy (Second Edition)*, Ferraro, J. R., Nakamoto, K., Brown, C. W. Eds.; Academic Press, 2003; pp 1-94.

43. Suh, J. S.; Moskovits, M. Surface-enhanced Raman spectroscopy of Amino Acids and Nucleotide Bases Adsorbed on Silver. *Journal of the American Chemical Society* **1986**, *108* (16), 4711-4718. DOI: 10.1021/ja00276a005.

44. Endrődi, B.; Kecsenovity, E.; Samu, A.; Halmágyi, T.; Rojas-Carbonell, S.; Wang, L.; Yan, Y.; Janáky, C. High Carbonate Ion Conductance of a Robust PiperION Membrane allows Industrial Current Density and Conversion in a Zero-gap Carbon Dioxide Electrolyzer Cell. *Energy & Environmental Science* **2020**, *13* (11), 4098-4105, 10.1039/D0EE02589E. DOI: 10.1039/D0EE02589E.

45. Yang, H.; Wu, Y.; Lin, Q.; Fan, L.; Chai, X.; Zhang, Q.; Liu, J.; He, C.; Lin, Z. Composition Tailoring via N and S Co-doping and Structure Tuning by Constructing Hierarchical Pores: Metal-Free Catalysts for High-Performance Electrochemical Reduction of CO_2. *Angew. Chem. Int. Ed.* **2018**, *57* (47), 15476-15480. DOI: https://doi.org/10.1002/anie.201809255.

46. Möller, T.; Ju, W.; Bagger, A.; Wang, X.; Luo, F.; Ngo Thanh, T.; Varela, A. S.; Rossmeisl, J.; Strasser, P. Efficient CO_2 to CO Electrolysis on Solid Ni–N–C Catalysts at Industrial Current Densities. *Energy & Environmental Science* **2019**, *12* (2), 640-647, 10.1039/C8EE02662A. DOI: 10.1039/C8EE02662A.

47. McCallum, C.; Gabardo, C. M.; O'Brien, C. P.; Edwards, J. P.; Wicks, J.; Xu, Y.; Sargent, E. H.; Sinton, D. Reducing the Crossover of Carbonate and Liquid Products During Carbon Dioxide Electroreduction. *Cell Reports Physical Science* **2021**, *2* (8), 100522. DOI: https://doi.org/10.1016/j.xcrp.2021.100522.

48.   Li, M.; Idros, M. N.; Wu, Y.; Burdyny, T.; Garg, S.; Zhao, X. S.; Wang, G.; Rufford, T. E. The Role of Electrode Wettability in Electrochemical Reduction of Carbon Dioxide. *Journal of Materials Chemistry A* **2021**, 10.1039/D1TA03636J. DOI: 10.1039/D1TA03636J.

49.   Garg, S.; Li, M.; Idros, M. N.; Wu, Y.; Wang, G.; Rufford, T. E. Is Maximising Current Density Always the Optimum Strategy in Electrolyser Design for Electrochemical CO_2 Conversion to Chemicals? **2021**.

Table of Contents